# Multiple wavelength reflectance microscopy to study the multiphysical behavior of microelectromechanical systems

N. Garraud,[1,2] Y. Fedala,[1,3] F. Kanoufi,[3] G. Tessier,[1] J. P. Roger,[1] and F. Amiot[4,*]

[1]*Institut Langevin, ESPCI ParisTech/CNRS-UMR 7587, 10 rue Vauquelin, 75231 Paris Cedex 05, France*

[2]*LMT-Cachan, ENS Cachan/CNRS-UMR 8535/Université Paris 6/PRES UniverSud Paris,*
*61 avenue du président Wilson, 94235 Cachan Cedex, France*

[3]*PECSA, ESPCI ParisTech/CNRS-UMR 7195, 10 rue Vauquelin, 75231 Paris Cedex 05, France*

[4]*FEMTO-ST Institute, CNRS-UMR 6174/UFC/ENSMM/UTBM, 24 chemin de l'Épitaphe, 25030 Besançon, France*
*\*Corresponding author: fabien.amiot@femto-st.fr*

In order to characterize surface chemomechanical phenomena driving microelectromechanical systems behavior, we propose herein a method to simultaneously obtain a full kinematic field describing the surface displacement and a map of its chemical modification from optical measurements. Using a microscope, reflected intensity fields are recorded for two different illumination wavelengths. Decoupling the wavelength-independent and -dependent contributions to the measured relative intensity changes then yields the sought fields. This method is applied to the investigation of the electroelastic coupling, providing images of both the local surface electrical charge density and the device deformation field.   © 2011 Optical Society of America

*OCIS codes:*   120.3930, 110.0180, 310.4925.

Because of their high surface over volume ratio, the mechanical behavior of micrometer-sized structures is significantly more surface-driven than that of usual macroscopic objects. This property has been proposed for use in devising micromechanical sensors of environmental changes [1]. In particular, a significant effort has been put into the development of biological sensors [2], thus highlighting the need for a more basic understanding of coupled surface phenomena [3]. Optical techniques, being nondestructive and allowing high spatial resolution, provide well suited tools.

In order to model chemically induced mechanical loadings, control of the chemical homogeneity of the considered surface is required. As surface chemical composition modifications induce complex reflection coefficient changes, Jin *et al.* [4] proposed an ellipsometric imaging setup to measure the optical thickness of thin adsorbed films. Li and White [5] also use interferometry to measure locally the concentration profiles of reactants near an electrode. Detections of differential reflectance changes have been achieved to perform sensitive electroreflectance [6] and thermoreflectance [7] measurements, providing access to electrochemically induced effects at substrate–electrolyte interfaces and surface temperature fields.

Modelling chemomechanical coupled phenomena also requires measuring kinematic fields of deformable surfaces. To measure cantilever profiles, Mertens *et al.* [8] propose a scanning optical lever technique. Several interferometric techniques have been proposed relying on phase changes related to the out-of-plane displacement field [9]. Optical lever and ellipsometric measurement techniques have been combined to monitor the mean surface curvature and global molecules adsorption on the surface of a microcantilever [10]. In order to obtain spatially resolved information, we propose to use multiple wavelength imaging reflection microscopy, which provides both local surface modification and kinematic field measurements. A decoupling method is presented to distinguish wavelength-dependent and -independent (i.e., kinematic) contributions to the collected intensity. The method is applied to the investigation of the electroelastic coupling on a cantilever beam, allowing one to simultaneously obtain an electroreflectance mapping and a field related to the local surface rotation of micrometer-sized structures.

To study coupled surface phenomena at the micrometer scale, deformable mechanical microcantilevers are subjected to time-dependent actuation. The objects under scrutiny are observed with an objective lens and imaged on a CCD array (Dalsa 1M30, 12 bits, $1024 \times 1024$ pixels; camera, I2S, France; lens, Olympus, France), using focusing optics (focal length 180 mm), as shown in Fig. 1(a). Reflected intensity changes arise either from surface reflectivity or from collection efficiency changes. The former is usually wavelength-dependent (as with electro- or thermoreflectance) while the latter is wavelength-independent, because it depends on the surface
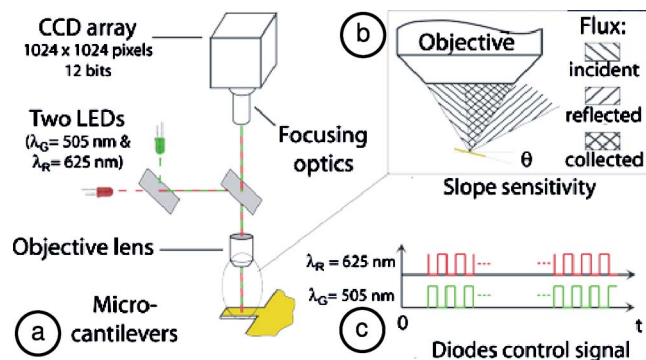


Fig. 1.   (Color online) a, Experimental setup with two sequentially triggered sources; b, sensitivity of the collected intensity to the surface orientation; c, light sources timing.

orientation and on the numerical aperture of the objective lens, which is corrected for chromatic aberrations [Fig. 1(b)]. In order to distinguish the wavelength-dependent and -independent contributions, the sample is illuminated with a green and a red LED of different wavelengths, namely, $\lambda_G = 505\,\text{nm}$ and $\lambda_R = 625\,\text{nm}$. These diodes are sequentially triggered by a 1.8 s period signal, provided by a function generator [Fig. 1(c)], and $N$ sums of 10 images are acquired for each illumination wavelength. The intensity, $I_m$, collected by the pixel, $P$, reads

$$I_m(P, \lambda, t_n) = I_i(P, \lambda) R(P, \lambda, t_n) \varepsilon(\theta(P), t_n), \qquad (1)$$

where $I_i(P, \lambda)$ is the intensity impinging on the surface conjugated with pixel $P$ at wavelength $\lambda$; $R(P, \lambda, t_n)$ is the reflectivity of the surface, i.e., the ratio of the reflected and incident intensities, depending on a local parameter, $X(P, t_n)$ (such as electrical charge, temperature, etc.) at the time step $t_n$. $\varepsilon(\theta(P), t_n)$ is the collection rate related to the local surface orientation, $\theta(P)$. The influence of $X(P, t_n)$ on the reflectivity is assumed to be small, so that $R$ is linearized:

$$R(P, \lambda, t_n) = R_0(P, \lambda)[1 + r(\lambda)X(P, t_n)], \qquad (2)$$

with $r(\lambda) = \frac{1}{R_0}\frac{\partial R}{\partial X}$ the relative reflectance sensitivity to the controlled parameter $X$. The geometrical effect $\varepsilon(\theta(P), t_n)$ is linearized in the case of small surface rotations around the initial orientation $\theta_0(P)$:

$$\varepsilon(\theta(P), t_n) = \varepsilon_0(\theta_0(P))[1 + d_{\theta_0}(P)(\theta(P, t_n) - \theta_0(P))], \quad (3)$$

with $d_{\theta_0}(P) = \frac{1}{\varepsilon_0}\frac{\partial \varepsilon}{\partial \theta}$ the local slope sensitivity. Finally, the measured intensity linearly depends on the wavelength-independent and -dependent relative intensity changes $R_{\text{wi}}(P, t)$ and $R_{\text{wd}}(\lambda, P, t)$, respectively:

$$I_m(P, \lambda, t_n) = I_a(P, \lambda)[1 + R_{\text{wd}}(\lambda, P, t_n) + R_{\text{wi}}(P, t_n)], \quad (4)$$

with

$$I_a(P, \lambda) = I_i(P, \lambda)R_0(P, \lambda)\varepsilon_0(\theta_0(P)),$$
$$R_{\text{wd}}(\lambda, P, t_n) = r(\lambda)X(P, t_n),$$
$$R_{\text{wi}}(P, t_n) = d_{\theta_0}(P)(\theta(P, t_n) - \theta_0(P)). \qquad (5)$$

For a given $(P, t_n)$, Eq. (4) is recast as the linear system

$$\begin{bmatrix} I_m(\lambda_R) - I_a(\lambda_R) \\ I_m(\lambda_G) - I_a(\lambda_G) \end{bmatrix} = \begin{bmatrix} I_a(\lambda_R) & I_a(\lambda_R) \\ kI_a(\lambda_G) & I_a(\lambda_G) \end{bmatrix} \begin{bmatrix} R_{\text{wd}}(\lambda_R) \\ R_{\text{wi}} \end{bmatrix}, \qquad (6)$$

where the ratio $k = r(\lambda_G)/r(\lambda_R)$ is assumed to be different from 1. The scalar, $k$, and the initial intensity fields, $I_a(P, \lambda)$, are obtained by preprocessing the data. Over the rigid substrate, $\Omega_s$, the local charge density, $X(P, t_n)$, is assumed to be equal to the mean charge density $X_i(t_n)$, so that at a given location, $I_a^{\text{sol}}(P, \lambda)$ is obtained as a minimizer (for a given set $\{c_q\}$) of the objective function $\eta^2(P, \lambda, I_a(P, \lambda), \{c_q\})$:

$$\eta^2(P, \lambda, I_a(P, \lambda), \{c_q\}) = \sum_{n=1}^{N}[I_m(P, \lambda, t_n)$$
$$- I_a(P, \lambda)f(X_i, \{c_q\})]^2, \qquad (7)$$

with

$$f(X_i, \{c_q\}) = 1 + \sum_{q=1}^{Q} c_q X_i^q(t_n). \qquad (8)$$

The coefficients $\{c_q\}$ are obtained as the minimizers of the sum $\kappa^2$ over $\Omega_s$ of the minimal $\eta^2$:

$$\kappa^2(\lambda, \{c_q\}) = \int_{P \in \Omega_s} \eta^2(P, \lambda, I_a^{\text{sol}}(P, \lambda), \{c_q\}). \qquad (9)$$

The coefficients $r(\lambda)$ are then obtained as the coefficient $c_1$ identified when considering a large area, $\Omega_s$. Repeating this procedure over the cantilever surface $\Omega_c$ (instead of $\Omega_s$), gathering all the pixels at a given abscissa along the cantilever axis then yields $I_a(P, \lambda)$ for these points. Values of $Q$ above 6 have been found to provide $r$ values independent of $Q$. Solving Eq. (6) then yields the relative intensity change contributions. The local slope sensitivity field, $d_{\theta_0}(P)$, is obtained by a calibration procedure to be detailed elsewhere.

The mechanical structures that were used are silica microcantilevers ($70\,\mu\text{m} \times 20\,\mu\text{m} \times 0.77\,\mu\text{m}$), covered with a 20 nm titanium adhesion layer and a 50 nm gold layer. These devices are placed in a cell and observed with an immersion objective lens ($\times 20$, NA 0.5). We focus here on the electromechanical effects induced by charging the gold surface. The cantilevers are immersed in a KCl electrolyte ($10^{-2}\,\text{mol.l}^{-1}$), and the electrical potential of their surface is controlled by an electrochemical workstation (CHI 660A, CH Instruments, USA) with respect to an Ag/AgCl reference electrode [11]. A total area of $A \simeq 50\,\text{mm}^2$ is in constant contact with the electrolytic solution. The gold surface is cleaned by varying its potential, $U_g$, from 0.1 to 0.8 V during three cycles at $12\,\text{mV.s}^{-1}$. Reference images are acquired, and the potential is then swept between 0.1 to 0.46 V at $4\,\text{mV.s}^{-1}$ while recording the electrode charge $A \times X_i$. $N = 50$ sums of 10 images are sequentially acquired for each wavelength during the cycle.

The preprocessing and decoupling procedure described above is applied to the recorded images, $I_m$ $(P, \lambda, t_n)$. The preprocessing yields $r(\lambda_R) = -162\,\text{cm}^2\,\text{C}^{-1}$ and $k = 2.03$, which is consistent with results in [12]. The calibration procedure also provides $d_{\theta_0}(P) \simeq 1\,\text{rad}^{-1}$ everywhere along the cantilever, so that the $R_{\text{wi}}$ and $R_{\text{wd}}(\lambda_R)$ fields are easily converted to a surface rotation (and thus a surface displacement) and local charge density fields, respectively. The signal-to-noise ratio can be improved by averaging $R_{\text{wi}}$ and $R_{\text{wd}}(\lambda_R)$ across the width of the beam. Figure 2 shows the evolution of the averages $\widetilde{R_{\text{wi}}}$ and $\widetilde{R_{\text{wd}}}(\lambda_R)$ as a function of time (vertical axis) along the axis of the beam (horizontal axis), which is anchored at $x = 0$.

$\widetilde{R_{\text{wi}}}$ does not vary on the substrate during the charging process, but increases up to $2 \times 10^{-3}$ because the
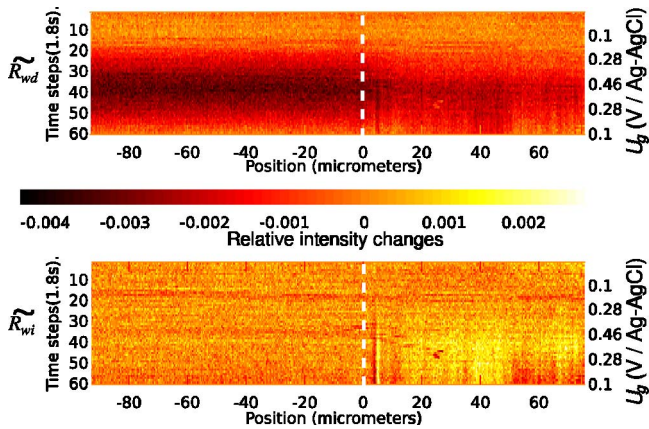
Fig. 2.   (Color online) Relative intensity changes $\tilde{R}_{\mathrm{wd}}(\lambda_R)$ (top) and $\tilde{R}_{\mathrm{wi}}$ (bottom) identified along the substrate ($x \leq 0$) and the beam ($x \geq 0$) during the loading cycle (time along the vertical axis). The cantilever is anchored at $x = 0$ (dashed line).



Fig. 3.   (Color online) Averages of $R_{\mathrm{wi}}$ and $R_{\mathrm{wd}}$ on the substrate and at the end of the beam versus the electrode charge $A \times X_i$. The solid lines are linear fits to each dataset. Calibrated values of the surface charge density (triangles) and surface rotation (circles) can be read on the right ordinate axis.

cantilever bends. This agrees with a mechanical effect acting only on deformable structures. $R_{\mathrm{wd}}(\lambda_R, P, t_n)$ is related to the local charge density, $X(P, t_n)$, and $R_{\mathrm{wd}}(\lambda_R)$, which is heterogeneous, decreases down to $-4 \times 10^{-3}$ on the substrate. In order to prove the electrochemical origin of the observed phenomena, Fig. 3 depicts the evolutions of $R_{\mathrm{wi}}$ and $R_{\mathrm{wd}}$ averaged on the whole substrate and at the edge of the cantilever (30% of its surface) as a function of the electrode charge $A \times X_i(t_n)$. Again, $R_{\mathrm{wi}}$ does not significantly change on the substrate (Fig. 3), which confirms its mechanical origin. All other evolutions are quasi-linear functions of the electrode charge, showing that the electrical charge density governs the mechanical effects and that the expansion [Eq.(2)] is valid. The $R_{\mathrm{wd}}$ contribution is twice as large on the substrate than at the cantilever's tip (Fig. 3), thereby proving that the charging process occurs heterogeneously along the cantilever. The deviation of $R_{\mathrm{wd}}$ obtained from the reference images yields an estimate of the standard deviation on the relative intensity changes: $\sigma_{R_{\mathrm{wd}}} \simeq 10^{-2}$ for a single pixel, which is reduced by spatial averaging to $\sigma_{\tilde{R}_{\mathrm{wd}}} \simeq 10^{-4}$.

The technique described here makes use of a standard reflection microscope with a CCD array and two sources of different wavelengths. Multiphysical phenomena occurring at their surfaces result in wavelength-dependent and -independent collected intensity variations, so that a procedure is proposed to decouple these contributions from intensity images at two different wavelengths. This method has been applied to microcantilevers under electrochemical actuation by varying the electrical potential of a substrate–aqueous electrolyte interface. The local charge density and rotation fields are obtained with a measurement reproducibility within the $10^{-4}$ range, thereby providing a powerful and simple way to study the multiphysical behavior of microelectromechanical systems devices.

### References

1. N. V. Lavrik, M. J. Sepaniak, and P. G. Datskos, Rev. Sci. Instrum. **75**, 2229 (2004).
2. J. Fritz, M. K. Baller, H. P. Lang, H. Rothuizen, P. Vettiger, E. Meyer, H.-J. Güntherodt, Ch. Gerber, and J. K. Gimzewski, Science **288**, 316 (2000).
3. M. F. Hagan, A. Majumdar, and A. K. Chakraborty, J. Phys. Chem. B **106**, 10163 (2002).
4. G. Jin, P. Tengvall, I. Lundström, and H. Arwin, Anal. Biochem. **232**, 69 (1995).
5. Q. Li and H. S. White, Anal. Chem. **67**, 561 (1995).
6. J. Feinleib, Phys. Rev. Lett. **16**, 1200 (1966).
7. G. Tessier, S. Holé, and D. Fournier, Appl. Phys. Lett. **78**, 2267 (2001).
8. J. Mertens, M. Álvarez, and J. Tamayo, Appl. Phys. Lett. **87**, 234102 (2005).
9. F. Amiot and J. P. Roger, Appl. Opt. **45**, 7800 (2006).
10. M. Godin, O. Laroche, V. Tabard-Cossa, L. Y. Beaulieu, P. Grütter, and P. J. Williams, Rev. Sci. Instrum. **74**, 4902 (2003).
11. F. Amiot, F. Hild, F. Kanoufi, and J. P. Roger, J. Appl. Phys. D **40,**, 3314 (2007).
12. R. Kofman, R. Garrigos, and P. Cheyssac, Thin Solid Films **82**, 73 (1981).